DFLDA - A MINIATURIZED, MOBILE LASER DOPPLER ANEMOMETER

Manfred Stieglmeier and Cam Tropea

Universität Erlangen-Nürnberg
Lehrstuhl für Strömungsmechanik
Cauerstr. 4, 8520 Erlangen, FRG

Abstract

A laser Doppler anemometer (LDA) has been developed which combines the compactness and low power consumption of laser diodes and avalanche photodiodes with the flexibility and possibility of miniaturization using fiber optic probes. The system has been named DFLDA for Diode Fiber LDA and is especially suited for mobile applications, for instance in trains, airplanes or automobiles. Optimization considerations of fiber optic probes are put forward and several probe examples are described in detail. Measurement results from two typical applications are given to illustrate the use of the DFLDA. Finally a number of future configurations of the DFLDA concept are discussed.

Introduction

The present work is an effort to combine the advantages of semiconductor elements in a laser Doppler anemometer (LDA) with those of fiber optic probes. The single-stripe, monomode laser diode offers substantial size reduction over conventional gas lasers and is available in commercially packaged form complete with correction optics and wavelength stabilization at power levels up to 100 mW[1]. Numerous laser-diode LDA systems have been developed and reported on in the past[2,3,4,5] however many of these systems have not offered directional sensitivity through some form of frequency shifting. Thus while the size of the system has been reduced in comparison with conventional gas laser systems they are of limited practical use. The addition of one or more Bragg cells[6], or the use of a rotating grating, immediately prohibits a miniaturization beyond the size of these frequency shifting elements. The use of fiber optic probes offers however the possibility of size reduction since the probe head can be made much smaller than the base optical unit, which can then be situated away from the actual measurement location. Not only can the probe head be made smaller but other advantages of fiber optic LDA probes can be exploited, for instance ruggedness, easier traversing and limited user adjustment. It will also be shown that probes of different sizes or configurations can easily be exchanged in such a system, increasing the overall flexibility of the system.

The DFLDA optical system will be described in the following section, giving first details of the base optical unit and then the fiber optic LDA probes. Several applications of the DFLDA are given in a further section, illustrating its ruggedness, mobility and ease of use. In the final section some possible extensions of the DFLDA concept using alternative components or probes, eg. for two-point velocity measurements, are outlined.

Description of the Optical System

Base Optical Unit

The base optical unit includes all optical components up to and including the fiber in-coupling as well as the avalanche photo diode (APD) for signal detection. While the main aim in designing this system is not to minimize the size, it should be kept small in light of the intended mobile applications (eg. in-flight measurements). More important is the ruggedness of the system, especially the fiber in-coupling as a high coupling efficiency must be maintained under a harsh mechanical environment (eg. train cars) and over a long duration in order to minimize user adjustment. The optical system developed for this purpose is illustrated schematically in Fig. 1 and pictured in Figs. 2 and 3. Its physical dimensions are 170 mm × 180 mm × 460 mm.

The laser source is a 100 mW single stripe monomode laser diode operating at 838 nm and packaged with a temperature regulation (±0.1° C), a correction optics for astigmatism and for achieving a circular beam profile[1]. The output power of this package is 94 mW and the beam is near circular with a diameter of 5.6 mm. This beam is collimated to a diameter of 1.2 mm with the beam waist positioned at the front face of the SELFOC lenses used for in-coupling. A passive optical isolator based on the Faraday effect is used to suppress reflections back into the laser diode and thus, any external resonator effects. Reflections are of particular concern when

CH3028-8/91/0000-0085 $1.00 © 1991 IEEE

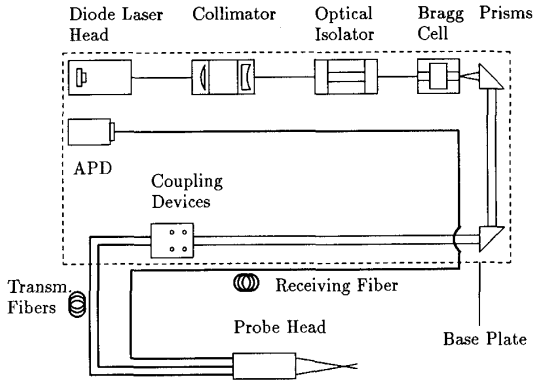

Figure 1: Block diagram of base optical unit with single Bragg cell

using fibers as they can be phase conjugate at the in-coupling surface where the phase fronts are plane. Without suppression of these reflections the laser diode experiences abrupt phase and power level variations[7] which are reflected in a smearing of the interference fringes in the measuring control volume, as shown in the photographs of Fig. 4. The beam power level after exiting the optical isolator is 88 mW.

The beam is split into two beams of equal intensity using the zeroeth and first order beams exiting from a Bragg cell (Matsushita EFL D 250 R) operated at 50 - 55 MHz. The intensity split is within $\pm$ 5 % with an overall efficiency in the two selected beams of $>$ 90 %. To keep the system compact and to allow the beams to separate in space, two prisms deflect the beams through 180° onto two in-coupling units (Polytec OFL-800). These units provide 4 axes of movement (2 translation, 2 tilt) and exhibit very high mechanical stability and repeatibility.

Figure 2: Photograph of DFLDA: cover removed

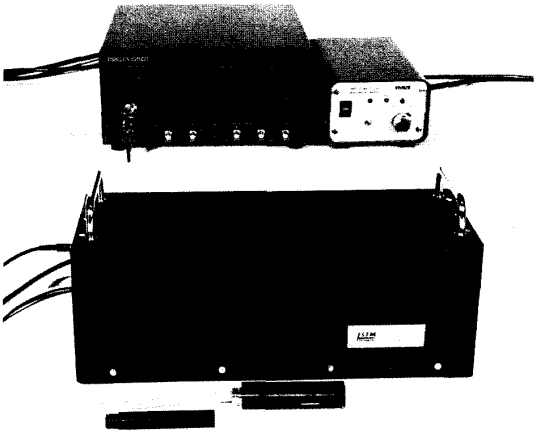

Figure 3: Photograph of DFLDA: assembled

a)

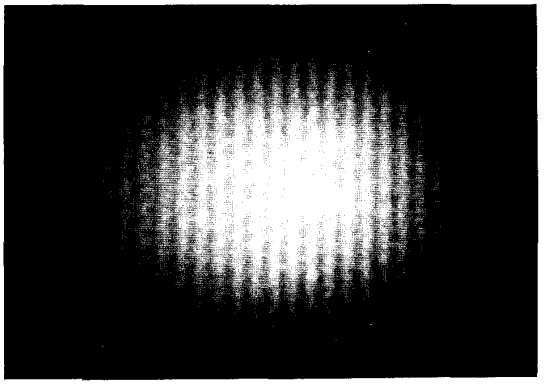

b)

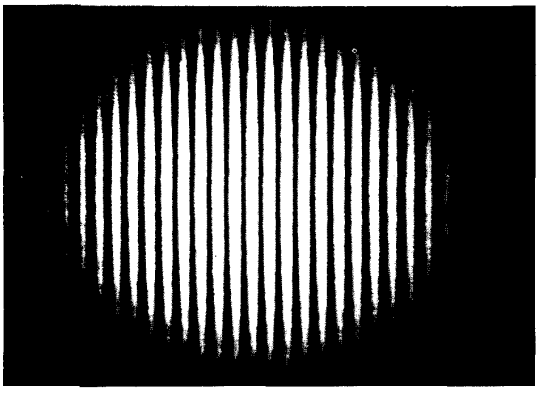

Figure 4: Image of fringes in measuring control volume (without shift) a) without optical isolator; b) with optical isolator

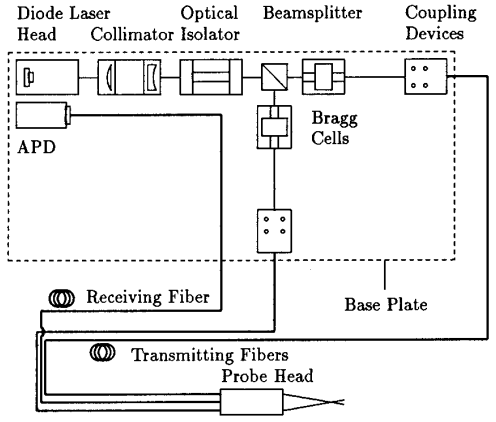

Figure 5: Block diagram of base optical unit with double Bragg cell

The in-coupling to the single-mode, polarization preserving (PANDA) fibers (Fujikura SM 85-P) is achieved using 1/4-pitch SELFOC lenses (NSG SLN 2.0 0.25 BC 0.83) butted directly against the polished fiber ends and held together in a glued ferrule. The beam diameter of 1.2 mm at the SELFOC front face results in a spot size of 5 μm, suitable for coupling into the PANDA fibers with a core diameter of 5.5 μm with transmission efficiencies exceeding 60 %.

This optical system results in a frequency shift of about 50 MHz, necessitating either a downmixing before processing or a processor of sufficient bandwidth. A second optical unit employing a beam splitter and two Bragg cells, as shown schematically in Fig. 5, allows more flexibility in the choice of shift frequency and is also more appropriate when the optics is being used as a transmission optics for a phase Doppler anemometer (PDA). In the present system a specially designed Bragg cell driver allows selection of the difference frequency over a range of 12 MHz with a resolution of 100 kHz. While the double Bragg cell system offers a higher degree of flexibility the physical size is larger (170 mm × 250 mm × 600 mm).

Probe Design

In the present work the size of the measuring probe was of importance and therefore some consideration was given to maximizing the collected scattered light intensity and hence, the signal-to-noise ratio (SNR) for a given probe diameter and focal length. Furthermore, only probes operating in the backscatter collection mode were considered.

The SNR can be related to system parameters by[8]

$$SNR \propto \frac{\eta \cdot P_0}{\Delta f} \left(\frac{D_a \cdot d_{in}}{f^2} \right)^2 a^2 \cdot G \cdot V^2 \qquad (1)$$

with a — particle diameter; D_a — receiving aperture; P_0 — input beam power; Δf — system bandwidth; G — scattering parameter; V — visibility; f — focal length; η — quantum efficiency of photodetector; d_{in} — beam diameter before front lens.

The optical factor

$$K = \left(\frac{D_a \cdot d_{in}}{f^2} \right)^2 \qquad (2)$$

will be termed an optical figure of merit and is determined solely by the layout of the measurement probe. Increasing this factor increases the SNR of the received signals.

The optical figure of merit K is interpreted as the product of two factors:

d_{in}^2/f^2 — to which the incident intensity in the measuring control volume (mcv) is proportional to and

D_a^2/f^2 — the square of the inverse aperture, to which the collected power is roughly proportional.

For a given probe diameter and a given focal length the optical figure of merit is therefore maximized by insuring that the receiving aperture (D_a) is as large as the probe diameter and by expanding the inlet beam before the front lens to increase d_{in}. The first requirement leads to receiving lenses with clearance holes for the outgoing beams, a customary design in commercial probes. As the beam diameter d_{in} is increased however, the clearance holes in the receiving lens must also increase in size, leading to a decrease in effective receiving aperture area. These mechanical constraints of a backscatter probe therefore lead to an optimization problem with regards to choosing the most effective beam expansion.

A Lorenz-Mie scattering program[9] was used further to investigate this optimization problem, i.e. the effect of increasing the beam diameter d_{in} while decreasing the receiving aperture due to the clearance holes. Calculations were performed for a 0.5 μm particle and the collected power was normalized with the collected power when the outgoing beam had a diameter of 1 mm. Results are shown in Fig. 6 for four different receiving aperture diameters. Note that these results are independent of focal length due to the normalization of the Y-axis. The beam diameter has been normalized with available clear aperture of the probe.

Fig. 6 is therefore a diagram of optical efficiency, expressing how efficient the optical layout uses the available probe diameter. These results indicate that the SNR continues to increase even beyond beam expansions which are no longer mechanically feasible ($d_{in}/D_a \sim 0.3$). Beyond this value the clearence holes in the receiving lens would be so large that the lens would consist of two parts. The conclusion of these

investigations is that, within mechanical feasibility, the beam expansion in the probe should be maximized.

One consequence of strong beam expansion is a smaller measuring control volume (*mcv*) and hence fewer real fringes, as also indicated in Fig. 6. This appears to be again a compromising situation since to measure a given velocity, a higher frequency shift is therefore required and this invariably lowers the effective accuracy of the processor in determining the Doppler frequency.

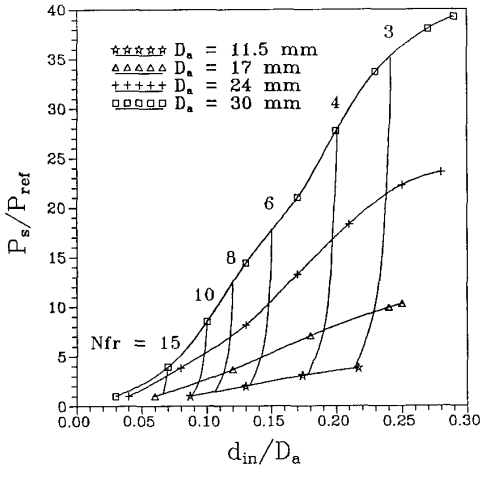

Figure 6: Normalized collected power as a function of normalized beam diameter for several receiving aperture diameters

Assuming the limiting (and hypothetical) case of no actual fringes in the *mcv*, the required frequency shift, f_{sh}, is given approximately by

$$f_{sh} = \frac{N_{min} \cdot |\vec{U}| \cdot \pi \cdot d_{in}}{4 \cdot f \cdot \lambda} \tag{3}$$

with N_{min} — minimum of number of periods in signal required by processor; $|\vec{U}|$ — magnitude of velocity vector. This illustrates the fact that a larger beam expansion requires a higher shift frequency. If this minimum shift frequency is always used and furthermore, a flow primarily perpendicular to the *mcv* fringes is assumed $|\vec{U}| = U_\perp$, a relative frequency error made by a counter processor due to the $\pm$ 1 timing count error can be derived as

$$\frac{\Delta f_D}{f_D} = \frac{N_{min}}{f_{osc} \cdot N_{fr}} \frac{U_\perp}{d_{mcv}} \tag{4}$$

with f_D — Doppler frequency corresponding to particle velocity; f_{osc} — oscillator frequency of counter time base; N_{fr} — number of real fringes in *mcv*; $U_\perp$ — flow velocity perpendicular to *mcv* fringes. Using values typical for a probe with strong beam expansion (s. table 1) (N_{min} = 8, U = 50 m/s, f_{osc} = 500 MHz, N_{fr} = 4, d_{mcv} = 20 μm) an error of less that 1 % is expected. This indicates that the probe optimization through beam expansion must not necessarily lead to serious errors in the signal processing because of smaller measuring volumes.

If the frequency shift is chosen independent of the optical parameters and held fixed, as in the present system, a more appropriate expression for the normalized frequency is given by

$$\frac{\Delta f_D}{f_D} = \frac{f_s^2}{N_{min} \cdot f_{osc}} \frac{1}{f_D} \tag{5}$$

where $f_s = f_{sh} + f_D$ is the signal frequency. Examination of this expression shows that the error will in general be larger. Using the parameter values given above with f_D = 5 MHz and f_{sh} = 50 MHz yields a relative error of 15 %. This error can be minimized by either increasing the minimum number of periods counted or by decreasing the shift frequency as much as possible, reaching in the limit the relative error given by Eq. 4. The reduction of shift frequency can be achieved either by electronic down-mixing or by using the double Bragg cell arrrangement described above.

It should be remarked that the relative error considered here due to a $\pm$ 1 timing count uncertainty in a counter processor is a statistical error with a mean of zero. This value expresses the smallest measurable frequency difference, i.e. the resolution. Other processors, for instance those based on a Fourier transform, should behave similarily since the accuracy of peak determination in a spectrum is approximately constant over the operating bandwidth[10] as is the counter $\pm$ 1 timing count uncertainty.

Description of the Probes

Using the considerations mentioned above, two fiber optic probes were constructed as shown in Fig. 7. The first probe is 19 mm in diameter and employes SELFOC lenses and a perforated negative lens to achieve beam expansion in a small probe diameter. A similar approach has been recently reported[11]. The second probe is 30 mm in diameter and uses microlenses to collimate the diverging beam after exiting the fibers and thus achieve a strong beam expansion. A summary of the optical specifications of these probes are given in Table 1 for various focal lengths. The operating conditions of these probes are also marked on Fig. 6, the 19 mm probe allowing a clear aperture of 15 mm and the 30 mm allowing a clear aperture of 24 mm.

Note that the optical figure of merit ranges between the values 1.8×10^{-6} and 1206×10^{-6} depending on the focal length used. Typical conventional LDA systems do not exceed values of 1 to 2 $\times 10^{-6}$ and optimized probes[11] achieved a value of 20 $\times 10^{-6}$. A further advantage of the present system, also

Probe Diameter (mm)	19			30			
Probe Length (mm)	104			115			
Front Lens Focal Length (mm)	36	60	100	60	120	200	250
Receiving Lens Focal Length (mm)	24 (48+48)			60			
Receiving Aperture Diameter (mm)	15			24			
Beam Separation (mm)	12			16			
Beam Diameter (mm)	3.0			3.5			
Number of Fringes (-)	5			6			
Half Intersection Angle (°)	9.46	5.71	3.43	7.60	3.81	2.29	1.83
Fringe Spacing (μm)	2.55	4.21	7.00	3.17	6.31	10.49	13.12
Diameter of *mcv* (μm)	13	21	35	19	37	61	76
Length of *mcv* (mm)	0.078	0.128	0.585	0.14	0.55	1.53	2.39
Optical Figure of Merit K ($\times 10^{-6}$)	1206	156	20	544	34	4.4	1.8

Table 1: Optical specifications of the 19 mm and 30 mm fiber optic probes

recognized in Eq. 1, is that the quantum efficiency of detection η of the avalanche photo diode (APD) at the operating wavelength of 838 nm is over 80 %, much higher than typical photomultipliers at visible wavelengths. Thus, the 35 mW – 40 mW present in the measuring control volume should be equivalent overall to many times this value in a conventional LDA system. Still a further advantage of the reduced control volume size, here between 13 μm and 76 μm, is the higher spatial resolution and the possiblity of near-wall measurements. This advantage will be illustrated in the following section.

Both of the probes pictured in Fig. 7 have interchangeable front lenses, allowing the focal length to be adjusted according to the application. The collected scattered light is focussed onto a graded-index multimode fiber (50/125 μm) and returned to an APD (INVENT APD 3.1) mounted in the base optical unit.

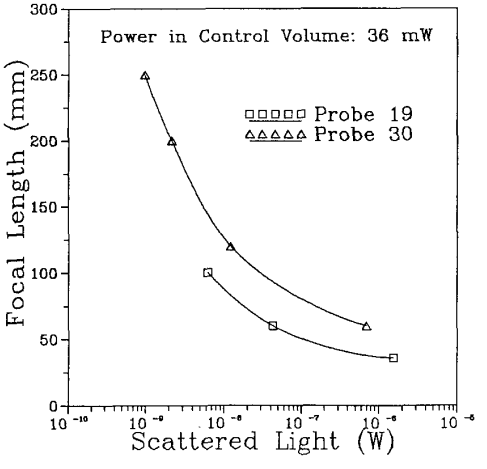

Figure 8: Computed power of collected scattered light for two probes (P_0 = 36 mW, d_{part} = 2 μm)

Probe 19

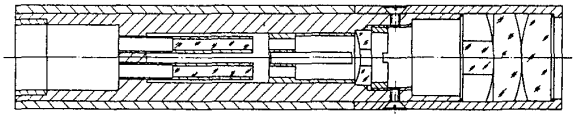

Probe 30

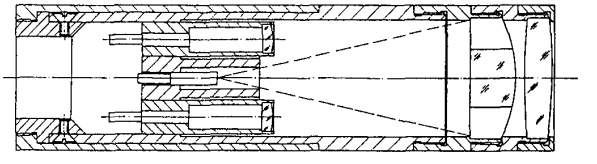

Figure 7: Cross-section views of the 19 mm and 30 mm fiber optic probes

The Lorenz-Mie scattering program was used to compute the collected scattered light intensity of these two probes for an incident light power of 36 mW and for a 2 μm water droplet centered in the *mcv*. The results of these computations are shown in Fig. 8. This diagram demonstrates that for a given focal length the 30 mm probe receives roughly four times higher scattered light powers than the 19 mm probe, consistent with the ratio of the optical figures of merit. The minimum required scattered light power for detection and evaluation has not been determined for this system, however signal quality is still high for $P_s = 10^{-9}$ mW.

Applications

During the development and testing phase of the diode fiber LDA (DFLDA) a large number of different flowfields have been investigated in widely differing operational environments. This extensive testing was considered essential to properly verify the system operation and to determine its practical capabilites, not only in terms of performance but also with respect to handling. Two of these applications are documented in the following sections.

In-Cylinder Measurements

In this application the flow velocity in a motored and fired four stroke research engine is measured with an angular resolution of 1 degree crank angle (CA). The research engine has been used previously[12] and was generously made available for the present study by the Institut für Motorenbau Prof. Huber (IMH) in Munich. Details of the engine are summarized in Table 2 and the measuring access window is illustrated in Fig. 9. Two velocity components were acquired sequentially, the radial and tangential component, as illustrated in Fig. 9. Although a nominal rotational speed of 1000 rpm is given in Table 2, experiments were also performed at 1500 rpm and 2000 rpm. Furthermore the engine was outfitted with a shrouded valve for these experiments.

A very important consideration in performing in-cylinder velocity measurements is the particle seeding. The particle seeding apparatus used in this facility is described fully in Lorenz and Prescher[13] and consists of a fluidized bed of TiO_2 particles mixed with hydrophobic Aerosil and injected with dryed (dew point -60°C) carrier air. The TiO_2 powder had a nominal particle size of 0.4 μm.

In the following experiment the (non-optimized) 30 mm fiber probe was used with a focal length of 60 mm ($K = 215 \cdot 10^{-6}$). The probe was mounted directly above the glass window and reached an equilibrium temperature of approximately 80°C during the experiments. No traversing was performed.

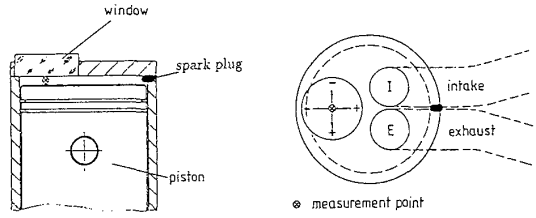

Figure 9: Measurement location and sign convention for in-cylinder velocity measurements

The single Bragg cell arrangement was used in the base optics with a frequency shift of 55 MHz. Processing was performed using a counter processor (TSI Inc., 1990) with a filter bandwidth of 5 MHz to 100 MHz. The data was acquired using a PC compatible laptop computer (Toshiba 5200) interfaced to the processor using a specially designed LDA data acquisition interface[14]. This interface also acquired the angular data for each processed Doppler burst. The processing was performed in 'single measurement/burst' mode with a minimum of 16 cycles and 1% comparison accuracy. All data shown in subsequent figures is *unaltered*, i.e. no procedure for removing bad data points has been implemented.

Initial tests were performed motoring the engine and some typical results are shown in Fig. 10. In Fig. 10a the radial and tangential velocity components at 1500 rpm are illustrated for a single cycle. Data rates averaged over the 4 strokes of up to 30,000 Hz were achieved, although 5,000 Hz - 6,000 Hz were more typical. The velocity traces shown in Fig. 10 are typical and agree qualitatively with unpublished data from IMH. Note that there are virtually no 'stray' data points requiring removal.

Experiments were continued under fired conditions and no observable difference in data rate could be detected. In both cases measurements could be performed over a longer period of time, ca. 2-3 min., representing 1000 - 3000 cycles de-

Dimensions					
Stroke	84	mm	Intake valve diameter	28	mm
Cylinder diameter	87	mm	Exhaust valve diameter	26	mm
Compression ratio	8.3		Window diameter	44	mm
Piston displacement	0.5	l	Combustion chamber	disk type	
Operating Parameters					
Rotational speed	1000	rpm	Intake valve lift	4.4	mm
Half load			Equivalence ratio λ_L	1.0	
Intake valve opening	710	° CA	Intake valve closing	253	° CA
Exhaust valve opening	486	° CA	Exhaust valve closing	11	° CA
Ignition before TDC	23	° CA	Fuel	Propane	

Table 2: Specifications and operating parameters of research engine

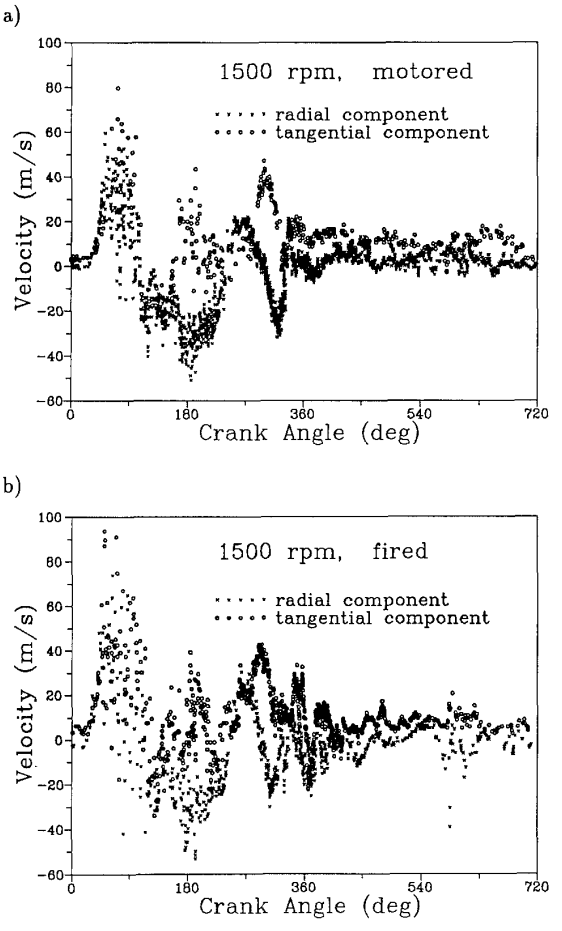

Figure 10: Typical single cycle velocity data in: a) motored engine; b) fired engine

pending on the rotational speed. Between experiments the window was removed and cleaned. In Fig. 10b the radial and tangential velocity components at 1500 rpm under fired conditions are shown for a single cycle.

The present results indicate that the DFLDA system is well-suited for in-cylinder flow investigations. Using the 19 mm probe, equivalent measurements should be possible using the 60 mm focal length. The observed signal quality was however very high, and while quantitative data is not available, measurements should also be possible at significantly longer focal lengths.

Mobile Application in Railroad Car

A further application field of the DFLDA is in aerodynamic studies, in this case the investigation of boundary layers on railroad cars. Tests were performed on two occasions, once with the Deutsche Bundesbahn (DB) and once with the SNCF (France). In the first instance a smoke generator operating on the principle of oil vaporization on a heated plate was used for seeding the railroad car boundary layer. This proved to be inappropriate, yielding low data rates and having the disadvantage of operating intermittantly. In the SNCF experiments an atomization of DES fluid using a commercial atomizer (TSI Inc., Model 9306) provided suitable particles. A portable compressor supplying air at 4 bar was used for the atomization. This arrangement yielded excellent results.

The double Bragg cell arrangement was used in the base optical system with a net frequency shift of 5 MHz. The 30 mm probe with focal lengths of 60 mm, 120 mm and 250 mm was used. An IFA-550 (TSI Inc.) signal processor was used for determination of the Doppler signal frequency and an acquisition interface and computer similar to those used in the engine measurements were used to acquire and process the data.

Measurements were made at several locations in a train car travelling at 100 km/h or 140 km/h, including a mid-section location and a location at the end of the car. The seeding probe could be placed up to one car upstream of the measurement location, however higher data rates were obtained when the seeding probe was closer to the measurement location. Although measurements could be made directly through the car window, the coating on the windows led to attenuation of the signals and therefore special plexiglass inserts were prepared at the desired measurement positions. A heavy optical tripod provided a traversing base for the probe inside the train car.

Some typical boundary layer profiles are illustrated in Fig. 11 for various measurement positions and train speeds. These profiles were obtained using the three different focal lengths, each lens used to measure in a different distance range from the window, up to a maximum distance of 23.5 cm. The overlap in profiles using different focal lengths is excellent despite the fact that the measurements were often performed many hours apart. Using the 60 mm focal length good measurements could be made up to 3 mm from the wall. At positions closer to the wall the shift frequency dominated the signal. This is primarily due to the vibration of the probe with respect to the window when the train is moving. Thus the window surface periodically enters the imaged control volume.

The prime reason for performing the measurements in the railroad car was to test the handling of the optics under adverse conditons. In this respect the optics performed excellently.

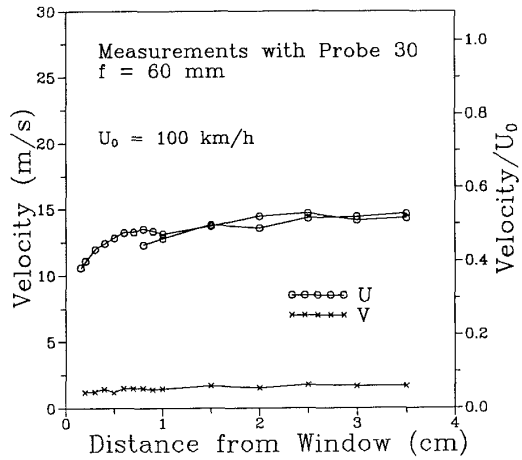

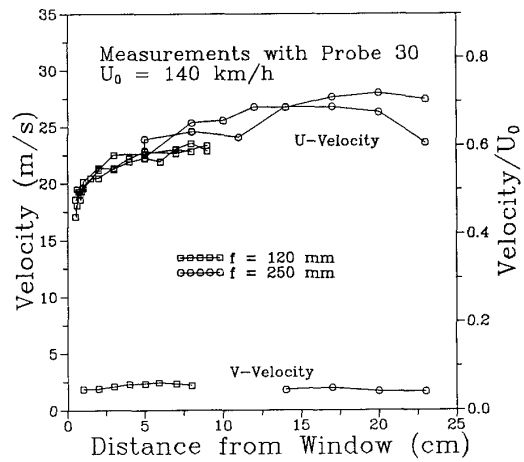

Figure 11: Typical boundary layer profiles using various focal lengths

Probe Diameter	(mm)	85		
Receiving Aperture	(mm)	80		
Beam Diameter	(mm)	5.0		
Focal Length	(mm)	150	310	500
K-Factor	($\times 10^{-6}$)	316	173	2.6

Table 3: Optical specifications of 85 mm probe

Future Developments

One major advantage of the DFLDA system is the ease with which probes can be exchanged. For instance a probe with 85 mm diameter has been designed for applications requiring longer focal lengths. Table 3 indicates that even for focal lengths of 500 mm the optical figure of merit can still exceed values typical of conventional systems.

In Fig. 12 a two-point probe is illustrated, based on the use of two 19 mm probes as described in section . Singlemode polarizing couplers are used to split the coupled light equally into two sets of fibers. The probes are then held in a positioner which allows adjustment of the position of the two control volumes. The incident light power in each individual probe is reduced, however Fig. 2 indicates that this power reduction factor of two will decrease the achievable focal length by only 16 %. Such a probe is presently being constructed to investigate the integral length scales in a compressing cylinder flow.

Higher laser powers is a second alternative to increasing the achievable focal lengths of the probes. Whereas 100 mW is expected to be the limit for single stripe monomode laser diodes, diode-pumped Nd:YAG lasers already provide 0.8 W at 1064 nm in commercially available packages. Presently the high cost of these lasers are a deterrent, as is the unavailability of fibers for this wavelength.

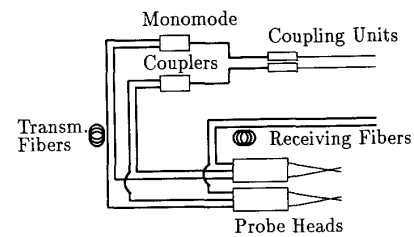

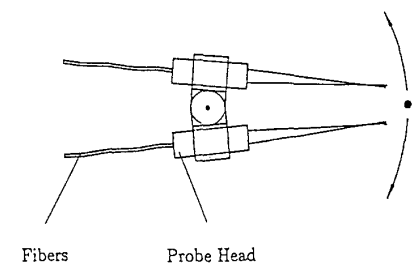

Figure 12: Two-point probe for the mesurement of space-time correlations

The extension of the DFLDA concept to two components is more complicated than with conventional Ar-Ion LDA systems since only one wavelength is available. Present designs forsee two solutions. The first is to use a second Bragg cell to introduce a third beam at a different shift frequency. A three or four beam system results, with bandpass filters used to separate the signals from a common detector. A second approach uses two base optical units with one laser diode at 838 nm and one Nd:YAG laser at 1064 nm or 532 nm (frequency doubled). Colour splitters and interference filters are then used to separate the signals from the two components.

The DFLDA system is suitable as a transmission optics for a PDA system. In this application it is desireable to also miniaturize the receiving optics and to employ fiber optics to yield a compact and mobile PDA probe. A DFPDA (Diode fiber PDA) is presently being constructed for this purpose[15].

Conclusions

The DFLDA concept has resulted in a measurement system which is superior to conventional LDA systems for moderate focal lengths (f < 250 mm). In addition the DFLDA has several advantages: compact, low power consumption, rugged for mobile use, lower cost and easy handling. The system is also of modular design, allowing easy replacement of individual components, such as laser diodes with higher powers or fiber optic probes for special applications.

References

[1] Melles Griot *Diode Laser Guide* Product Catalogue.

[2] Dopheide, D., Faber, M., Reim, G., Taux, G. 1988 *A Portable Frequency Stabilized Laser Diode Backscatter Semiconductor LDA for High Velocity Applications* Proc. 4th Int. Symp. on Appl. of Laser Anemometry to Fluid Mech., Lisbon.

[3] Müller, R., Naqwi. A. 1988 *Optimization of a Laser Diode Anemometry System* Report LSTM 239/T/88, Lehrstuhl für Strömungsmechanik, Universität Erlangen-Nürnberg.

[4] Brown, R.G.W., Burnett, J.G., Hackney. N. 1988 *A Miniature, Battery Operated Laser Doppler Anemometer* Proc. 4th Int. Symp. on Appl. of Laser Anemometry to Fluid Mech., Lisbon.

[5] de Mul, F.F.M., Jentink, H.W., Koelink, M., Greve, J. Aarnoudse, J.G. 1989 *Velocimetry with Diode Lasers* Third Int. Conf. Laser Anemom.- Advances and Appl., Swansea.

[6] Polytec GmbH *Laserdiode LDA* Product Information.

[7] Goldberg, L., Taylor, H.F., Dandrige A., Weller, J.F., Miles, R.O. 1982 em Spectral Characteristics of Semiconductor Lasers with Optical Feedback IEEE Trans. on Microwave Theory and Techniques **MTT-30** No. 4 401-420.

[8] TSI Inc. *Laser Doppler Velocimetry ; Components* Product Catalogue.

[9] Naqwi, A. Durst, F. 1989 *Computation of Light Scattering from a Dual-Beam System* Report LSTM 259/T/89 Lehrstuhl für Strömungsmechanik, Universität Erlangen-Nürnberg.

[10] Tropea, C., Dimaczek, G., Kristensen, J. 1988 *Evaluation of the Dantec Burst Spectrum Analyzer* Report LSTM 218/I/1988, Lehrstuhl für Strömungsmechanik, Universität Erlangen-Nürnberg.

[11] Ikeda, Y., Nakajiwa, T., Hosokawa, S., Matsumoto, R. 1990 *A Compact Fiber LDV with a Perforated Beam Expander* Meas. Sci. Technol. **1** 260-264.

[12] Bopp, S., Durst, F., Tropea, C. 1990 *In-Cylinder Velocity Measurements with a Mobile Fiber Optic LDA System* SAE Paper 900055, Society of Automotive Engineers.

[13] Lorenz, M., Prescher, K. 1990 *Cycle Resolved LDV Measurements of a aFired SI-Engine at High Data Rates Using a Conventional Modular LDV-System* SAE Paper 900054, Society of Automotive Engineers.

[14] Tropea, C., Struthers D. 1987 *Microprocessor Based On-line Measurement System for LDA* Proc. Use of Computers in Laser Anemometry, Saint Louis France.

[15] Domnick, J., Tropea, C., Wagner, R., 1991 *A Miniaturized Semiconductor Fiber Optic Phase-Doppler Anemometer (SFOPDA) with Applications to Liquid Sprays*, Int. Conf. on Multiphase Flows 1991, Tsukuba, Japan.